HHS Public Access

Author manuscript

Neuron. Author manuscript; available in PMC 2015 August 07.

Published in final edited form as:

Neuron. 2013 June 5; 78(5): 895–909. doi:10.1016/j.neuron.2013.03.030.

Temporal and mosaic *Tsc1* deletion in the developing thalamus disrupts thalamocortical circuitry, neural function, and behavior

Elizabeth A. Normand[1], **Shane R. Crandall**[1], **Catherine A. Thorne**[1], **Emily M. Murphy**[1], **Bettina Voelcker**[2], **Catherine Browning**[2], **Jason T. Machan**[3], **Christopher I. Moore**[1], **Barry W. Connors**[1], and **Mark Zervas**[2,*]

[1]Department of Neuroscience, Division of Biology and Medicine, Brown University, 70 Ship St., Providence, RI 02903

[2]Department of Molecular Biology, Cell Biology and Biochemistry, Division of Biology and Medicine, Brown University, 70 Ship St., Providence, RI 02903

[3]Departments of Orthopedics and Surgery at Rhode Island Hospital and the Warren Alpert Medical School at Brown University, Providence, Rhode Island 02903

SUMMARY

Tuberous Sclerosis is a developmental genetic disorder caused by mutations in *TSC1*, which results in epilepsy, autism, and intellectual disability. The cause of these neurological deficits remains unresolved. Imaging studies suggest the thalamus may be affected in Tuberous Sclerosis patients, but this has not been experimentally interrogated. We hypothesized that thalamic deletion of *Tsc1* at distinct stages of brain development would produce differential phenotypes. We show that mosaic *Tsc1* deletion within thalamic precursors at embryonic day (E)12.5 disrupts thalamic circuitry and alters neuronal physiology. *Tsc1* deletion at this early stage is unique in causing both seizures and compulsive grooming in adult mice. Only a subset of these phenotypes occurs when thalamic *Tsc1* is deleted at a later embryonic stage. Our findings demonstrate that abnormalities in a discrete population of neurons can cause global brain dysfunction and that phenotype severity depends on developmental timing and degree of genetic mosaicism.

Keywords

Tuberous Sclerosis; Tsc1; mTOR; thalamus; neurodevelopment; vibrissa barrels; seizures; repetitive grooming; mosaicism

*Correspondence should be addressed to M.Z.: Laboratory of Developmental Neurobiology, Genetics and Neurological Disease, Department of Molecular Biology, Cell Biology and Biochemistry, Division of Biology and Medicine, Box G-E436, Brown University, Providence, RI 02912, Courier delivery: Laboratories for Molecular Medicine, 70 Ship Street, Rm. 436, Providence, RI 02903, Mark_Zervas@brown.edu, Tel: 401-863-6840, Fax: 401-863-9653, Web page: http://research.brown.edu/myresearch/Mark_Zervas.

INTRODUCTION

Tuberous Sclerosis (TS) is a complex mosaic genetic disorder that affects one in 6000 children and commonly presents in infancy or early childhood, suggesting an early developmental basis for the disease. TS is characterized by benign hamartomas in multiple organs, but neurological involvement is common and debilitating. Patients may experience seizures (70–90%), intellectual disability (50%), autism (25–50%), and sleep disturbances (McClintock, 2002). Hamartomas in the brain were thought to cause the neurological symptoms, but the extent of hamartomas does not necessarily correlate with the severity of neurological impairment (Wong and Khong, 2006). This suggests that subtle aspects of brain development or function are perturbed in TS.

Genetically, TS is caused by mutations in either of two tumor suppressor genes, *TSC1* or *TSC2*, and is inherited in an autosomal dominant manner. In addition to the inherited mutation, a somatic mutation in the remaining functional allele results in loss of heterozygosity and gives rise to isolated *TSC*-null cells that proliferate and contribute to the formation of hamartomas (Au et al., 1999). This “two-hit” mechanism results in a mosaic population of cells in a patient’s organs: a discrete population that has undergone a second hit to become null for *TSC1* or *TSC2*, and surrounding heterozygous cells. However, it is unclear whether this two-hit mechanism underlies neurocognitive aspects of TS (Crino et al., 2010). To experimentally emulate this mosaic state within the brain and to test whether targeted disruption of *Tsc1* in a focal manner can disrupt global brain function, we employed an inducible CreER/*loxP*-based method of gene inactivation in mice, which produces a spatially restricted, mosaic population of *Tsc1*-mutant cells surrounded by genetically unaffected cells.

The TSC1 and TSC2 proteins form a heterodimer that negatively regulates the mTOR pathway, which in turn modulates a wide array of cellular processes (Hay, 2004). The multifaceted nature of the mTOR pathway raises the possibility that the effects of *TSC* loss-of-function vary depending on a cell’s identity, functional role, or developmental state at the time of *TSC* mutation. During brain development cell fate specification, cell growth, differentiation, and axonal connectivity are tightly regulated to establish proper brain architecture and function. Thus, spatially and temporally controlling *Tsc1* deletion in targeted cell types and comparing the resulting phenotypes will instructive to our understanding of this complex disease. Because our CreER/*loxP* experimental system is temporally inducible, we are able to target *Tsc1* inactivation to distinct stages of brain development.

Numerous studies have evaluated how *Tsc1/2* deletion affects the cerebral cortex. Subcortical regions have not been extensively evaluated thus far, although one such structure that warrants investigation based on previous findings is the thalamus. MRI-imaging studies of TS patients show changes in thalamic gray matter volume that correlates with poor cognitive performance (Ridler et al., 2006). Thalamic involvement in TS is relevant because the thalamus provides all specific, information-carrying afferents to the cerebral cortex and plays a crucial role in higher order cognitive processes (Saalmann and Kastner, 2011). The thalamus also projects robustly to the striatum, a pathway implicated in

attentional orientation (Smith et al., 2004). Notably, dysfunction of the thalamus and striatum are implicated in obsessive compulsive disorder and autism (Hardan et al., 2008; Fitzgerald et al., 2011). The relay cells of the thalamus receive extensive excitatory feedback from the neocortex, and inhibitory inputs from the thalamic reticular nucleus (TRN). Due, in part, to this extensive reciprocal connectivity, the thalamus plays a key role in oscillatory neocortical dynamics and in the generation of low-frequency rhythms, which are prominent in specific forms of epileptic activity (Blumenfeld, 2003). We have used spatially and temporally controlled *Tsc1* gene deletion to address how altered thalamic development has the potential to perturb widespread neural function and behavior.

RESULTS

Spatiotemporal contribution of the *Gbx2 lineage* to adult thalamic neurons

To temporally and spatially control *Tsc1* gene deletion, we combined three genetically-modified mouse alleles (Figure S1A): 1. $Gbx2^{CreER}$, which targets CreER expression to thalamic cells (Chen et al., 2009); 2. $Tsc1^{fl}$, which is converted into a null allele ($Tsc1^{\Delta}$) by Cre-mediated recombination (Kwiatkowski et al., 2002); 3. either $R26^{LacZ}$ (Soriano, 1999) or $R26^{tdTomato}$ (Madisen et al., 2010), which produce β-galactosidase (β-gal) or red fluorescent protein (RFP), respectively, upon Cre-mediated recombination. CreER remains quiescent until it is transiently activated by tamoxifen. Subsequently, the $Tsc1^{fl}$ gene is permanently converted to $Tsc1^{\Delta}$ and the conditional reporter genes are permanently activated in the thalamus (Figure S1). $Gbx2^{CreER}$ expression has been reported in the spinal cord (Luu et al., 2011) but, within the brain, regions outside of the thalamus had virtually no recombination at E12.5 (Figure S1). We validated the fidelity of $Tsc1^{fl}$ recombination in the thalamus compared to the neocortex (Figure S1D). Operationally, we use $Tsc1^{\Delta E12/\Delta E12}$ to indicate mutant animals that received tamoxifen on embryonic day (E) 12.5 and $Tsc1^{\Delta E18/\Delta E18}$ to indicate mutants that received tamoxifen on E18.5. We first performed genetic inducible fate mapping on $Gbx2^{CreER};R26^{LacZ}$ animals to characterize the extent, spatial distribution, and molecular identity of recombined (Figure 1). We administered tamoxifen to pregnant females carrying $Gbx2^{CreER};R26^{LacZ}$ embryos at E12.5 or E18.5 and determined the long term lineage contribution to the thalamus. Postnatal brain sections were analyzed by immunohistochemistry (IHC) for β-gal expression from the activated $R26^{LacZ}$ allele. E12.5 fate-mapped cells (green) were distributed widely throughout the full medial-lateral extent of the thalamus (Figure 1A–F). In animals that received tamoxifen at E18.5, the spatial extent of recombination was reduced (Figure 1G–L). Regions that underwent recombination at both E12.5 and E18.5 include the anteromedial and mediodorsal nuclei. The ventrolateral, ventromedial, ventrobasal, and the lateral geniculate nuclei underwent recombination at E12.5, but were not marked at E18.5. Nuclei that underwent extensive recombination early (E12.5) and moderate mosaic recombination later (E18.5) include the posterior nucleus and the medial geniculate nucleus. We investigated whether recombination occurred in a particular cell type by IHC for β-gal in combination with parvalbumin (PV, red, Figure 1A–C,G–I) or calbindin (Calb, red, Figure 1D–F,J–L). Within relay nuclei, β-gal + cells contributed to both Calb- and Calb+ cells at both E12.5 and E18.5 (Figure 1D–F, J–L, arrowheads). Although most excitatory relay neurons did not express any PV+ within their soma, there were a few examples of neurons with low PV+ levels that also expressed β-

gal at E12.5 (Figure1A–C, arrowheads). Notably, the PV+ inhibitory thalamic reticular nucleus (TRN) did not undergo recombination at either stage.

mTOR pathway dysregulation occurs rapidly after *Tsc1* recombination

We used the inducible nature of our system to control the timing of *Tsc1* gene deletion and determine how rapidly mTOR dysregulation occurs. We administered tamoxifen to E12.5 embryos with $Gbx2^{CreER}$ and either $Tsc1^{+/+}$ or $Tsc1^{fl/fl}$. E12.5 is a stage when thalamic neurons have differentiated and are beginning to extend axonal projections toward the cortex (Molnár et al., 1998). We compared mTOR activity in the $Tsc1^{+/+}$ and $Tsc1^{\Delta E12/\Delta E12}$ *thalamus* at E14.5 by IHC for the S6 protein phosphorylated at Ser240/244 (pS6), which is a reliable readout of mTOR pathway activity. We observed basal pS6 expression in the E14.5 $Tsc1^{+/+}$ brain (Figure 2A), consistent with the requirement for mTOR activity during early development (Hentges et al., 2001). Nevertheless, in the E14.5 $Tsc1^{\Delta E12/\Delta E12}$ thalamus, there was an increase in thalamic pS6 levels over controls (Figure 2B). In E17.5 $Tsc1^{\Delta E12/\Delta E12}$ embryos, thalamic levels of pS6 were also dramatically increased compared to controls (Figure 2C–D). These experiments show, for the first time, how rapidly neurons respond to *Tsc1* gene inactivation *in vivo* during embryogenesis. mTOR dysregulation persisted in the postnatal $Tsc1^{\Delta E12/\Delta E12}$ thalamus but was negligible in the $Tsc1^{+/+}$ and $Tsc1^{+/\Delta E12}$ controls (Figure 2E–G). $R26^{LacZ}$ reporter activation (β-gal, green) validated that all genotypes had a similar extent of CreER-mediated recombination. Similar results were seen with IHC for pS6(Ser235/236), another mTOR-dependent S6 phosphorylation site (data not shown).

E12.5 *Tsc1* deletion alters morphology and circuitry in mature thalamic neurons

To determine whether mTOR dysregulation affected morphology of adult thalamic neurons, we quantified soma size based on the somatodendritic marker, microtubule-associated protein 2 (MAP2). Sections were also stained for pS6 (red). CreER-mediated recombination produced mTOR dysregulation in 70% of thalamic neurons in $Tsc1^{\Delta E12/\Delta E12}$ mice (621 out of 878 MAP2+ neurons). We took advantage of this mosaicism and sorted neurons into two populations: dysregulated $Tsc1^{\Delta E12/\Delta E12}$ neurons (pS6+, filled arrowheads) and unaffected neurons (pS6-, open arrowheads, Figure 3B). The geometric mean soma area of pS6+ $Tsc1^{\Delta E12/\Delta E12}$ neurons was 403μm, significantly larger than $Tsc1^{+/+}$ (220μm^2), $Tsc1^{\Delta E12/+}$ (209μm^2), and pS6- $Tsc1^{\Delta E12/\Delta E12}$ neurons (220μm^2) (p=0.003, n=3 mice per genotype, Figure 3B, see Table S1 for variability estimates). Because normal-sized pS6- cells neighbored enlarged pS6+ cells, we conclude that neuron overgrowth occurs in a cell-autonomous manner. We also detected substantial PV expression in fibers within the internal capsule of $Tsc1^{\Delta E12/\Delta E12}$ brains (Figure 3E'), which was absent in controls (Figure 3C'). Because corticothalamic and thalamocortical axons (TCAs) intermingle in the internal capsule we assayed for $R26^{tdTomato}$ expression. RFP/PV co-localization in the fibers (Figure 3C,E) and cell bodies of thalamic relay neurons (Figure 3D,F) confirmed that the PV+ signal was from the $Tsc1^{\Delta E12/\Delta E12}$ TCAs. Because previous TS mouse models have described myelination defects and astrocytosis (Meikle et al., 2008; Way et al., 2009; Carson et al., 2012), we assayed for myelin basic protein (MBP) and glial fibrillary acidic protein (GFAP). Control mice had clear MBP labeling throughout the brain, including within the thalamus and the internal capsule, and this did not differ between mutants and controls (Figure S2).

Only sporadic GFAP+ cells were observed in the thalamus of both mutants and controls. Because the enlarged *Tsc1* $^{\Delta E12/\Delta E12}$ thalamic neurons were reminiscent of dysmorphic neurons in neuronal storage disorders, we assayed for GM2 ganglioside, which accumulates in these disorders (Zervas et al., 2001). GM2 was not detected in *Tsc1*$^{+/+}$ or *Tsc1*$^{\Delta E12/\Delta E12}$ thalamic neurons (data not shown).

We next investigated whether deleting *Tsc1* at E12.5 affected thalamocortical circuit development. We took advantage of the highly organized and stereotyped projections from the thalamic ventrobasal nuclear complex (VB) to the vibrissa barrels in layer IV of primary somatosensory cortex (SI) (Woolsey and Van der Loos, 1970). We used *R26*^{tdTomato} to label thalamic projections for neural circuit analysis. In control animals, TCAs innervated layer IV of somatosensory cortex in discrete clusters corresponding to individual vibrissae (Figure 4A, region 1), similar to descriptions using non-genetic labeling (Wimmer et al., 2010). In contrast, *Tsc1*$^{\Delta E12/\Delta E12}$ mice had a diffuse pattern of cortical innervation: individual barrels were indistinguishable in layer IV (Figure 4B, region 1) and projections were overabundant in the deep layers (arrow). Within the internal capsule, TCA fascicles appeared less sharply defined compared to controls (Figure 4A,B region 2). We confirmed these findings by stereotaxic injection of lentiviral-GFP into VB in control and mutant animals (Cruikshank et al., 2010), which filled infected neurons with GFP, including their axons and terminal projections (Figure S3).

To assess the effect of the disorganized TCAs on genetically normal cortical targets, we used cytochrome oxidase (CO) staining, which is enriched in the dendritic mitochondria of layer IV spiny stellate barrel neurons (Wong-Riley and Welt, 1980) and nicely delineates the barrel hollow structures (Figure 4C–J). In controls, RFP+ TCAs were enriched in the CO+ barrel hollows and largely excluded from the surrounding septa (Figure 4E, asterisks and arrowheads, respectively). In *Tsc1*$^{\Delta E12/\Delta E12}$ mutants the TCAs were not only localized to barrel hollows (Figure 4I, asterisks), but were also heavily distributed throughout the septal regions (arrowheads). The CO staining pattern was also altered in *Tsc1*$^{\Delta E12/\Delta E12}$ brains, suggesting that the cortical barrels were improperly patterned (Figure 4, compare C,D to G,H). The small vibrissa barrels were particularly indistinct in the *Tsc1*$^{\Delta E12/\Delta E12}$ cortex (Figure 4D,H, gray regions), which was a phenotype reminiscent of that described in *mGluR5* knockout mice (She et al., 2009). To quantitatively assess the large barrels (Figure D,H, orange regions), we outlined the limits of the SI vibrissa region and the individual barrels based on CO staining in a genotype-blinded manner. The average barrel size was larger in mutants (58mm^2) compared to controls (37mm^2, $p<0.001$, n>72 barrels across 3 mice per genotype, two-sample two-tailed t-test; Figure 4K). Quantification of the septal proportion of the barrel region based on CO staining showed no significant difference between *Tsc1*$^{\Delta E12/\Delta E12}$ (21%) and controls (25%, p=0.16, n=3 mice per genotype, two-sample two-tailed t-test; Figure 4L). To determine whether the organization of the cortical cell bodies was altered, we combined NeuN antibody labeling with CO staining to quantify cell density in the barrel hollows (outer limit of the CO+ barrel hollow is indicated by the dashed lines in Figure 4F,J) and the surrounding barrel wall region (indicated by the solid lines in Figure F,J) (Narboux-Neme et al., 2012). Mutants had lower neuron density in the barrel wall region (3.7 neurons/mm^2) than controls (Figure 4M; 4.5 neurons/mm^2). This

same trend applied to the barrel hollow region (*Tsc1*$^{\Delta E12/\Delta E12}$ 3.2 neurons/mm^2; *Tsc1*$^{+/+}$ 3.5 neurons/mm^2, $p_{wall}<0.001$, $p_{hollow}=0.020$, n≥20 non-adjacent barrels across 3 animals per genotype, two-sample two-tailed t-test; Figure 4M). Together, these experiments confirmed that thalamic *Tsc1* inactivation causes mTOR dysregulation, cell overgrowth, aberrant PV expression, and altered thalamocortical projections that affect the genetically normal neocortex.

Later deletion of *Tsc1* causes more subtle cellular changes than those arising from early inactivation

We administered tamoxifen at E18.5 to compare the effects of thalamic *Tsc1* inactivation at a later developmental stage. By E18.5, thalamic neurons have fully differentiated, their axonal projections have accumulated in the subplate of their cortical target regions, and they are beginning to invade the cortical layers (Molnár et al., 1998). Upon reaching adulthood, *Tsc1*$^{\Delta E18/\Delta E18}$ brains were analyzed for mTOR activity and cell size (Figure 5A). mTOR was dysregulated in 29% of neurons (221 out of 542 MAP2+ cells) in the *Tsc1*$^{\Delta E18/\Delta E18}$ thalamus, as evidenced by increased pS6 (Figure 5A). We analyzed cell size as described in Figure 3. Although some pS6+ *Tsc1*$^{\Delta E18/\Delta E18}$ neurons skewed toward larger cell sizes than pS6- neurons, on average, pS6+ *Tsc1*$^{\Delta E18/\Delta E18}$ neurons (359μm^2) were not significantly larger than pS6- *Tsc1*$^{\Delta E18/\Delta E18}$ (246μm^2), *Tsc1*$^{\Delta E18/+}$ (242μm^2), or *Tsc1*$^{+/+}$ cells (253μm^2, p=0.11; Figure 5A). We observed rare pS6+ neurons in the *Tsc1*$^{+/+}$ (2 out of 632 cells, average size 304μm^2, data not shown) and *Tsc1*$^{\Delta E18/+}$ thalamus (8 out of 1069 cells, average size: 277μm^2), which are not graphed for clarity. Unlike the E12.5 findings, aberrant PV expression was not apparent in either axons or cell bodies of *Tsc1*$^{\Delta E18/\Delta E18}$ thalamic neurons (Figure 5B,C region 3, data not shown). *Tsc1*$^{\Delta E18/\Delta E18}$ thalamocortical projections appeared coarse within the internal capsule and overabundant within deep cortical layers (Figure 5B,C arrows), similar to the E12.5 findings. Because of the different recombination pattern, the vibrissal barrel-projecting neurons in VB did not undergo recombination and thus were not labeled by the *R26*^{tdTomato} reporter. For this reason, TCA innervation of the vibrissa barrels could not be visualized by RFP expression. Nevertheless, we assessed vibrissa barrel formation using CO staining, which showed that the *Tsc1*$^{\Delta E18/\Delta E18}$ somatosensory cortex did not have any patterning disruptions (Figure S4).

Intrinsic physiology is abnormal in *Tsc1*$^{\Delta E12/\Delta E12}$, but not *Tsc1*$^{\Delta E18/\Delta E18+}$, thalamic neurons

To interrogate the functional effects of *Tsc1* deletion on individual cells at E12.5 versus E18.5, we performed whole-cell patch-clamp recordings on thalamic VB neurons (Figure 6). (For all data in this section, see Supplemental Table 1 variability estimates, non-significant means and p-values.) We recorded from VB because it is easily identifiable and its relay neurons exhibit stereotyped, well-characterized physiological properties (Landisman and Connors, 2007). We used RFP fluorescence from the *R26*^{tdTomato} reporter allele to target our recordings to recombined neurons. Biocytin was added to the recording pipette to identify neurons post-hoc, reconstruct their morphology, and confirm mTOR dysregulation in mutant neurons (Figure 6A). We characterized the intrinsic membrane properties of *Tsc1*$^{\Delta E12/\Delta E12}$ and *Tsc1*$^{\Delta E18/\Delta E18}$ VB neurons compared to neurons from their respective *Tsc1*$^{+/+}$ littermates. *Tsc1*$^{\Delta E12/\Delta E12}$ VB neurons had significantly lower input resistance than neurons in *Tsc1*$^{+/+}$ littermates (72.6 MΩ versus 137.2 MΩ, p =0.001; Figure 6B). In addition,

Tsc1$^{\Delta E12/\Delta E12}$ VB neurons had a higher capacitance than *Tsc1*$^{+/+}$ neurons (417.6 pF versus 219.7 pF, p=0.004, Figure 6B). In contrast, *Tsc1*$^{\Delta E18/\Delta E18}$ neurons did not differ from their controls in either resistance or capacitance (Figure 6B). The membrane time constant was unchanged in *Tsc1*$^{\Delta E12/\Delta E12}$ and *Tsc1*$^{\Delta E18/\Delta E18}$ compared to controls (Figure 6B), because the decrease in resistance offset the increase in capacitance.

We also analyzed the properties and dynamics of action potentials in VB neurons (Figure 6C). Action potential thresholds in *Tsc1*$^{\Delta E12/\Delta E12}$ neurons were similar to those of *Tsc1*$^{+/+}$. However, *Tsc1*$^{\Delta E12/\Delta E12}$ neurons, when compared to *Tsc1*$^{+/+}$ neurons, had significantly larger spike amplitude (82 mV versus 70 mV, p=0.0002), and faster rates of depolarization (618 mV/ms versus 423 mV/ms, p=0.0001), and repolarization (−263 mV/ms versus −151 mV/ms, p<0.0001). *Tsc1*$^{\Delta E18/\Delta E18}$ spikes did not differ significantly from those of *Tsc1*$^{+/+}$ neurons in terms of amplitude, depolarization rate, or repolarization rate. VB action potentials are typically followed by fast and slow after-hyperpolarizations (AHPs) and an after-depolarization (ADP) of intermediate duration (Figure 6D, black trace). To compare these events we summed the total area under the post-action potential trajectory, which revealed that the *Tsc1*$^{\Delta E12/\Delta E12}$ neurons had significantly more negative after-potentials compared to controls (−177 mV·ms versus −64 mV·ms, p=0.0026; Figure 6D). The *Tsc1*$^{\Delta E78/\Delta E18}$ after-potentials did not differ significantly from controls (Figure S5).

Thalamic relay neurons fire in both tonic and bursting modes, depending on the state of the resting membrane potential. We characterized tonic firing by holding the membrane potential at −50mV and applying steps of depolarizing current. While the amplitudes of *Tsc1*$^{+/+}$ action potentials declined over the first 100 ms of spiking (adaptation), the amplitudes of *Tsc1*$^{\Delta E12/\Delta E12}$ action potentials remained constant (Figure 6E, arrows). The relationship between firing frequency and stimulus current was roughly linear for both *Tsc1*$^{+/+}$ and *Tsc1*$^{\Delta E12/\Delta E12}$ cells (Figure 6F). The average slope of the frequency/current relationship for *Tsc1*$^{\Delta E12/\Delta E12}$ cells (0.27 Hz/pA) was significantly lower than that of *Tsc1*$^{+/+}$ cells from littermate controls (0.52 Hz/pA, p<0.001, n≥11 cells recorded from n≥3 animals per group; Figure 6G). Frequency/current relationships of *Tsc1*$^{\Delta E18/\Delta E18}$ cells did not differ from those of littermate controls (Figures 6G and S5). We next characterized the cells' burst firing by holding membrane potentials initially at −60 mV, then injecting a 1 sec step of current sufficient to bring the membrane to −70 mV. Upon release of the current, VB neurons fired a single burst of spikes (Figure 6H). Each burst comprised a similar number of action potentials that did not vary by genotype, however the mean duration of the *Tsc1*$^{\Delta E12/\Delta E12}$ bursts were shorter. Figure 6I plots the intra-burst frequency as a function of spike number within the bursts; *Tsc1*$^{\Delta E12/\Delta E12}$ neurons had a significantly higher mean spiking frequency throughout the burst (400 Hz) compared to *Tsc1*$^{+/+}$ littermate controls (mean of 339 Hz, p=0.026). *Tsc1*$^{\Delta E18/\Delta E18}$ neurons were not significantly different from neurons of *Tsc1*$^{+/+}$ littermates (Figures 6J and S5). These experiments revealed that the enlarged *Tsc1*$^{\Delta E12/\Delta E12}$ neurons require stronger input currents to modify their membrane potentials, have larger, faster action potentials, and have altered firing properties in both tonic and bursting mode, compared to wildtype VB neurons, whereas *Tsc1*$^{\Delta E18/\Delta E18}$ neurons were unaltered.

Thalamic *Tsc1* deletion at E12.5 and E18.5 causes abnormal neural activity and behavior

To determine whether the changes in thalamic development and physiology impact neocortical physiology, we recorded local field potentials (LFP) in the vibrissal representation of primary somatosensory cortex (SI) of anesthetized mice. We chose SI because it receives robust input from VB, where we detected changes in circuit organization and whole-cell physiology. We confirmed targeting to barrel cortex by stimulating vibrissae to drive sensory-evoked responses (data not shown). We observed prominent low-frequency oscillations in both $Tsc1^{\Delta E12/\Delta E12}$ and $Tsc1^{\Delta E18/\Delta E18}$ mice (Figure 7A–C, n=6 $Tsc1^{+/+}$, n=3 $Tsc1^{\Delta E12/\Delta E12}$, n=5 $Tsc1^{\Delta E18/\Delta E18}$ mice). Quantitative analysis of LFP activity showed that mutants had higher power across multiple frequencies, particularly in the 3 Hz range (Figure 7D). This is a frequency associated with spike-and-wave epileptiform activity, which is related to altered thalamic dynamics (Blumenfeld, 2003). Mutants had significantly higher 3 Hz power than controls (p=0.008, Figure 7E), which was evident in the comparison across all individuals (controls in black, mutants in pink/red triangles). Further, the number of epochs of high-power 3Hz activity lasting ≥ 20 seconds was significantly higher in $Tsc1^{\Delta E12/\Delta E12}$ (red triangles) and $Tsc1^{\Delta E18/\Delta E18}$ mutant animals (pink triangles) compared to controls (p=0.028, Figure 7F). Older (>8 months) $Tsc1^{\Delta E18/\Delta E18}$ animals and controls were also assessed to account for possible age-related differences in brain activity. These data points are differentiated by black outlines in panels E and F.

We addressed whether there were any behavioral ramifications of this altered brain activity. At two months of age, $Tsc1^{\Delta E12/\Delta E12}$ mice seemed to groom more frequently than control littermates and developed severe skin lesions (Figure 7G, inset). Because control littermates never developed lesions, but were housed in the same cage as affected mice, we hypothesized that the lesions were due to the excessive self-grooming, rather than environmental factors, fighting, or allo-grooming. Importantly, over-grooming was apparent before wounds developed, indicating that the wound was not the trigger for the grooming, but rather a result of it. To confirm this, animals were videotaped for 8-minute periods twice a week in their homecage before wounds appeared. An observer scored the amount of time spent grooming by each mouse in a genotype-blinded manner. $Tsc1^{\Delta E12/\Delta E12}$ mice spent significantly more of their time grooming (24.1%, 95% confidence interval (CI_{95}): 21.8 − 26.5%) than $Tsc1^{+/+}$ (3.0%, CI_{95}: 2.4 − 3.9%) and $Tsc1^{\Delta E12/+}$ mice (3.8%, CI_{95}: 3.0 − 4.9%, p<0.0001, n≥11 mice per genotype; Figure 7G). In contrast, $Tsc1^{\Delta E18/\Delta E18}$ mice displayed no overt phenotypes by 3 months of age (n=17) and did not develop wounds or groom more often than $Tsc1^{+/+}$ or $Tsc1^{\Delta E18/+}$ littermates, regardless of age (n=25 and n=6 respectively, Figure 7G).

$Tsc1^{\Delta E12/\Delta E12}$ mice also exhibited spontaneous seizures beginning around 2 months of age, consistent with the increase in 3Hz LFP activity. The seizure events were highly stereotyped and began with prolonged grooming of the hindlimb, followed by loss of upright posture, then a tonic-clonic state during which the body entered into a convulsive, twisted posture typically lasting 10 seconds (Figure 7H, inset; Supplemental Video 1). An observer blinded to genotype quantified the frequency and duration of seizures. The $Tsc1^{\Delta E12/\Delta E12}$ mice averaged 3.7 seizures/hour (CI_{95}: 2.0 − 6.9 seizures/hour), while control littermates never exhibited seizures (Figure 7H). 91% of the $Tsc1^{\Delta E12/\Delta E12}$ mice (10/11) that were analyzed

experienced convulsive seizures as described above during the observation periods. While the remaining mouse did not have overt seizures, it did display abnormal behavior in that it remained in a motionless, sleep-like state for minutes at a time, which may have been absence seizures. In contrast, *Tsc1*$^{\Delta E18/\Delta E18}$ mice did not exhibit seizures at 2 months of age. However, by 8 months of age, 4 of the 17 *Tsc1*$^{\Delta E18/\Delta E18}$ mice had experienced a seizure (Figure 7H), but these rare seizure events only occurred upon handling. Thus, we conclude that 100% of *Tsc1*$^{\Delta E12/\Delta E12}$ mice and 24% of *Tsc1*$^{\Delta E18/\Delta E18}$ mice displayed abnormal behavior, with some variation in form and severity. Notably, the severity of the grooming and the seizure phenotypes was not correlated within individuals.

Because *Gbx2*^{CreER} mediates recombination in the spinal cord at E12.5 (Luu et al., 2011), we tested peripheral sensory and motor function (Figure S6). We did not detect a significant difference in tactile sensitivity (von Frey filament test, p=0.315) or motor function (wire hang assay, p=0.134) between control and *Tsc1*$^{\Delta E12/\Delta E12}$ animals. We also showed that thermal pain sensitivity was unaffected in *Tsc1*$^{\Delta E12/\Delta E12}$ mutants (hot plate test, p=0.188). Because *Gbx2*^{CreER} is no longer expressed in the spinal cord after E14.5 (John et al., 2005), we did not perform similar tests on *Tsc1*$^{\Delta E18/\Delta E18}$ animals. Taken together, our collective analysis of thalamocortical circuitry, neuronal physiology and neocortical local fields potentials strongly suggest that the primary drive of these *Tsc1*$^{\Delta E12/\Delta E12}$ or *Tsc1*$^{\Delta E18/\Delta E18}$ phenotypes is mTOR dysregulation in the thalamus.

DISCUSSION

TS is a developmental mosaic genetic disorder caused by disrupting the TSC/mTOR pathway. In this study, we tested the hypothesis that disrupting the mTOR pathway elicits different phenotypes depending on the identity and developmental state of cells in which *Tsc1* is deleted and mTOR is dysregulated.

Genetic circuit tracing showed that *Tsc1*$^{\Delta E12/\Delta E12}$ thalamic projections are disorganized and have excessive processes that innervate layer IV septal regions of the somatosensory barrel cortex. This phenotype may result from the lack of activity-dependent pruning or excess axonal ramifications filling intra-barrel spaces, consistent with previous reports describing abnormal axonal targeting of retinal projections in both the *Drosophila* and mouse brain, where *Tsc1* mutant axons overshoot their target, and have branches that terminate outside the normal target regions (Knox et al., 2007; Nie et al., 2010). It is probable that other cortical areas receive similarly disorganized *Tsc1*$^{\Delta E12/\Delta E12}$ thalamic inputs. We also analyzed *Tsc1*$^{\Delta E18/\Delta E18}$ TCA projections as they traversed the striatum and entered the cortex. Similar to *Tsc1*$^{\Delta E12/\Delta E12}$, there was a qualitative excess of RFP+ *Tsc1*$^{\Delta E18/\Delta E18}$ TCA projections within the deep cortical layers. However, a direct comparison of *Tsc1*$^{\Delta E18/\Delta E18}$ and *Tsc1*$^{\Delta E12/\Delta E12}$ vibrissa barrel innervation was precluded because of their different recombination patterns. Regardless, these thalamocortical projection phenotypes in deep layers are consistent with disrupted neuronal processes in response to mTOR dysregulation (Choi et al., 2008).

We uncovered multiple electrophysiological alterations upon early deletion of *Tsc1*. The increased input capacitance and reduced input resistance are both consistent with increased

membrane as a result of cell growth. Notably, action potential dynamics were also altered, yet spike threshold potentials were unaffected. The altered action potentials of *Tsc1*$^{\Delta E12/\Delta E12}$ neurons may partially compensate for the changes in passive properties. As the input resistance of a neuron falls, larger synaptic currents are required to modify membrane voltage. However, mutant *Tsc1*$^{\Delta E12/\Delta E12}$ neurons have larger amplitude, briefer action potentials with normal thresholds and rates of rise and fall that are considerably faster than normal. The maximum rate-of-rise of an action potential is proportional to peak inward sodium current in many neurons (Cohen et al., 1981). Therefore, these changes in spike kinetics strongly suggest that voltage-gated sodium and potassium channels are altered in the mutant cells. The spike shapes are consistent with either higher membrane channel densities or altered single-channel properties, such as subunit composition or phosphorylation, that affect conductance and gating dynamics. In support of these possibilities, the mTOR pathway has been reported to control expression levels and subunit composition of some voltage-gated ion channels (Raab-Graham et al., 2006). Multiple ion channel involvement is further suggested by changes in both the tonic and burst-firing modes of mutant cells. The reduced slope of the tonic frequency/current relationship in mutant cells is most easily explained as a consequence of their lower input resistance. More rapid intra-burst spiking is likely due to changes in ion channels; in addition to altered spike-related sodium and potassium channels, it is possible that the rapid intra-burst spiking in *Tsc1*$^{\Delta E12/\Delta E12}$ cells is caused by altered density or kinetics of low-threshold calcium channels. Additionally, the ectopic production of PV, a protein that acts as a slow Ca^{2+} buffer, in *Tsc1*$^{\Delta E12/\Delta E12}$ thalamic relay neurons may disrupt internal Ca^{2+} dynamics, which can affect gene transcription, synaptic function, and membrane potential and could contribute to some of the physiological changes we describe (Schwaller, 2010).

Importantly, our data show that the effects of early mutation spread well beyond the cells with the *Tsc1* deletion. Individually mutated neurons ensnare the neocortex into hyperexcitable networks, as evidenced by abnormal LFPs in SI. Thus, disruption of a single node of anatomically disparate but functionally connected regions can propagate the disease phenotype. Comparing the effects of early and late *Tsc1* deletion is informative. We did not detect abnormal physiological properties of *Tsc1*$^{\Delta E18/\Delta E18}$ VB neurons, which indicates that, at least for VB neurons, there is a critical window of *Tsc1/mTOR* required to establish proper intrinsic excitability properties. Nevertheless, a striking finding is that neocortical (SI) LFP activity was altered in some E18.5-deletion animals. The most parsimonious reason for the global abnormalities is that feedback loops involving multiple thalamic nuclei have altered physiology, which is propagated both locally and to other brain regions. The sources of altered feedback may involve thalamic nuclei that undergo extensive recombination at E18.5 (such as Po) and that subsequently disrupt the reticulo-thalamic or the cortico-thalamic loops. By comparing the early versus later deletion of *Tsc1* we are able to discern that abnormalities, even in a small proportion of cells, can cause reverberating global changes in neural activity.

Comparison of our thalamic *Tsc1* mutant phenotypes to other mouse models can be informative in considering the contribution of individual brain regions to global neural dysfunction. Behaviorally, *Tsc1*$^{\Delta E12/\Delta E12}$ animals groomed excessively, to the extent that

they gave themselves severe lesions. A similar over-grooming phenotype has been described in genetic mouse models of autism and obsessive compulsive disorder in which *Slitrk5, Shank3* or *Sapap3* is deleted (Welch et al., 2007; Shmelkov et al., 2010; Peça et al., 2011). Because striatum-specific gene rescue can ameliorate the phenotype, these groups implicate the corticostriatal circuit in causing abnormal repetitive behaviors. The thalamus projects both directly (Smith et al., 2004) and indirectly, via neocortex, to the striatum, suggesting that abnormal thalamic modulation of the striatum in our mice contribute to the repetitive grooming phenotype. However, it is possible that sparse recombination in other subcortical brain structures, such as the striatum and hindbrain, may also contribute to the behavioral changes. *Tsc1* or *Tsc2* knockout in Purkinje cells of the cerebellum also causes repetitive grooming (Tsai et al., 2012; Reith et al., 2013), possibly by disrupting signals from the cerebellum to the motor cortex, which are relayed by the ventrolateral thalamus. In addition, all $Tsc1^{\Delta E12/\Delta E12}$ and some $Tsc1^{\Delta E18/\Delta E18}$ mice experience seizures and abnormal neural activity with epileptiform features. Seizures are a common feature of TS clinically. *Tsc1* knockout in forebrain neurons leads to seizures in 10% of mice (Meikle et al., 2007), while *Tsc1* deletion in astrocytes (and likely neurons as well (Casper and McCarthy, 2006)) causes frequent seizures and premature death (Uhlmann et al., 2002). Widespread deletion of *Tsc1* in neural progenitors has also been shown to cause spontaneous seizures in adult mice (Goto et al., 2011). Ours, however, is the first conditional *Tsc1* knockout to cause both seizures and over-grooming. Although one may presume that this is simply because the thalamus is a central structure and its dysregulation therefore compromises multiple functional circuits, the explanation cannot be that simple; in the Meikle et al and Goto et al studies, *Tsc1* recombination occurs in the thalamus as well as the rest of the forebrain. The fact that more comprehensive *Tsc1* knockouts do not produce similar over-grooming suggests that perturbing a single node of a neural network has the potential to be more deleterious than disrupting the entire network, perhaps because global homeostatic mechanisms are not invoked when only part of a highly interconnected and integrative system is dysregulated. This is an important consideration for brain structures, such as the thalamus, which feature complex feedback loops and widespread reciprocal connectivity that could amplify and spread the effects of a slight functional imbalance. This concept is particularly relevant given the mosaic nature of TS in humans, in which subsets of cells undergo biallelic *TSC1/2* mutations, leading to discrete cohorts of mutant cells (Crino et al., 2010). It is important to note, however, that while thalamic *Tsc1* knockout replicates some features of TS, we are not implying that TS is a disease of the thalamus. Rather, our findings suggest that the thalamus and other subcortical regions warrant further investigation, and that the complex nature of disorders like TS involve multiple brain regions that may respond differentially to the same genetic insult.

The phenotypes related to E12.5 versus E18.5 *Tsc1* inactivation suggest three contributing factors: the spatial pattern of recombination, the overall number of affected cells, and the developmental timing of *Tsc1* inactivation. The spatial pattern of recombination is clearly important and experimentally arises from the dynamic expression of the *Gbx2* gene regulatory elements that drive *CreER* expression (Chen et al., 2009). The dynamic recombination pattern causes the MD, MG and AM nuclei to undergo recombination at both E12.5 and E18.5. In contrast, the Pf and VB nuclei are virtually spared by recombination at

E18.5. This differential involvement of nuclei likely leads to distinct consequences. The Pf and VB nuclei project, either directly or indirectly, to the dorsolateral striatum (Pan et al., 2010), which is a central component in a circuit that regulates a syntactic chain of grooming behaviors (Cromwell and Berridge, 1996). Disruption of this circuit at E12.5, but not at E18.5, could underlie the compulsive grooming behavior in $Tsc1^{\Delta E12/\Delta E12}$, but not $Tsc1^{\Delta E18/\Delta E18}$, mutant animals. Alternatively, there may be a threshold extent of mosaicism that can be tolerated and compensated for by the brain, above which compensatory mechanisms become ineffective. In this regard, the lower overall number of recombined cells in the $Tsc1^{\Delta E18/\Delta E18}$ thalamus might place the system near the tolerance threshold, resulting in abnormal neural activity, but with only a subset of animals experiencing overt seizures, and only during external stimulation. In contrast, the extensive recombination within the $Tsc1^{\Delta E12/\Delta E12}$ thalamus may be above the tolerance threshold, resulting in unmitigated disruption of thalamic development and function. Finally, because mTOR regulates many developmental cellular programs including proliferation, cell growth, axon formation, synapse formation and maintenance, it is also possible that the later deletion of *Tsc1* results in a diminished phenotype simply because there is a critical period during which thalamic neurons require functional *Tsc1*. By E18.5, thalamic neurons have already extended their axons to their cortical target regions so this developmental event would be spared when *Tsc1* inactivation occurs at E18.5, but may be affected by earlier *Tsc1* inactivation. This idea is consistent with the fact that, at the single-cell level, recombined VB neurons display aberrant protein expression and altered electrophysiological properties when recombination occurs at E12.5, while VB neurons are apparently unaffected when recombination occurs at E18.5.

It is likely that all three of these factors—the specific cells that suffer the genetic insult, the number of cells that are affected, and the developmental stage at which the genetic hit occurs—contribute to the distinct E12.5 and E18.5 phenotypes to some degree. Although this complex interplay of multiple factors precludes making simple conclusions about mechanisms, it does nicely mimic the complex nature of mosaic disorders such as TS. Mosaic genetic diseases can have extremely variable penetrance, expressivity, and severity. The factors that can contribute to this disease variability, similar to those in our mouse model, include: when during development the initial genetic mutation occurs, in which cell that mutation happens (and how the affected gene functions in that cell type), and how extensively that initial cell's lineage contributes to the final organism (Hall, 1988). Our temporally and spatially controllable mouse model of TS allows us to manipulate where and when the *Tsc1* gene is deleted, which is instructive in understanding the consequences of mosaic genetic insults at distinct stages of development. Future studies that further parse the contributions of these factors will be instrumental for understanding the developmental underpinnings and mechanisms that contribute to Tuberous Sclerosis and to mosaic diseases in general.

EXPERIMENTAL PROCEDURES

Mice, Tissue Processing, and Cellular Analysis

Tsc1^{fl} *Rosa26*$^{loxP\text{-}STOP\text{-}loxP\text{-}LacZ}$ (*R26*^{LacZ}), *R26*$^{loxP\text{-}STOP\text{-}loxP\text{-}tdTomato}$ (*R26*^{tdTomato}) and *Gbx2*$^{CreER\text{-}IRES\text{-}eGFP}$ mice (*Gbx2*^{CreER}) mice were described previously (Soriano, 1999; Kwiatkowski et al., 2002; Chen et al., 2009; Madisen et al., 2010). Mice were housed and handled in accordance with Brown University Institutional Animal Care and Use Committee guidelines. Genotyping, tamoxifen, immunohistochemistry (IHC), antibodies, and cytochrome oxidase (CO) staining are described in Supplemental Experimental Procedures. Identical exposure settings were used when comparing labeling intensity across the three genotypes. For neuron density analysis, a barrel outline was created based on CO+ staining ("barrel hollow") and a perimeter was made 15μm outside the inner outline ("barrel wall"). The area and the number of NeuN-positive objects in the barrel hollow and wall regions were determined analyzed for significance by Student's t-test. For cell size analysis, five thalamic regions from five medial-to-lateral brain sections were assessed. The Measure function was used to calculate the perimeter and area of all outlined cell bodies. Generalized Estimating Equations (log-normal generalized model) were used to compare genotypes with regards to neuronal size. Pair-wise comparisons were made using orthogonal contrast statements, with p-values adjusted using the Holm test to maintain family-wise alpha at 0.05. Statistical and experimental details are provided in Supplemental Experimental Procedures.

Whole-cell Recordings

Brain slice preparation, solutions, and recording conditions (Cruikshank et al., 2012) are provided in detail in Supplemental Experimental Procedures. Data were collected with Clampex 10.0 and analyses were performed post-hoc using Clampfit 10.0. Resting membrane potentials (R_m), input resistances (R_{in}), and membrane time constants (τ_m), and input capacitances (C_{in}) were determined as described in Supplemental Experimental Procedures. Burst properties were characterized by holding the soma at a membrane potential of −60 mV with intracellular current and subsequently injecting large negative currents. Tonic and single action potential properties were characterized by holding the soma at a membrane potential of −50 mV with intracellular current and injecting suprathreshhold positive current. Single action potential data were obtained by injecting the minimum current needed to elicit an action potential. After-hyperpolarizations (AHPs) were evoked by injecting a 2 ms suprathreshold positive current. Generalized Hierarchical Linear Modeling was use to test for differential effects of gene deletion. Comparisons by genotype were made using orthogonal linear comparisons.

LFP Recordings

Surgical procedures, recordings, and analysis are described in Supplemental Experimental Procedures. NeuroNexus probes were used for recording sessions. Local field potential (LFP) signals were sampled, filtered, and recorded using a Cheetah Data Acquisition System (NeuraLynx). The probe was lowered 1600μm and responses to vibrissa deflections confirmed electrode placement in SI. Ten minutes of pre- and post-baseline activity and a stimulus period was recorded. Inter-trial periods had a mean period of 5 seconds. For each

animal, a single SI recording session was selected for LFP analysis using the layer IV contact. Recorded signals were low-pass filtered, downsampled, and clipping artifacts were removed. Data were analyzed using Matlab. The power spectral density (PSD) for 20-second non-overlapping time windows was estimated using Welch's method with a 4096-point FFT, normalized by dividing by the sum of the PSD across all frequencies, and smoothed using a 5-pt moving average filter. Relative power at 3 Hz was calculated as the ratio of the normalized PSD at 3 Hz by the value at 1 Hz for each time window, averaged across the session. The number of 20-second windows that exceeded 97.5th percentile of normalized 3 Hz power was counted. Two-tailed two-sample t-tests were performed by grouping all controls versus all mutants (significance level, α of 0.05).

Behavioral Analysis

An independent observer assessed videos to score seizures and over-grooming as detailed in Supplemental Experimental Procedures. Generalized Estimating Equations were used to compare genotypes with regards to percent minutes grooming (binomial generalized model grooming/total minutes) and seizure frequency (negative-binomial generalized model offset by log total hours). Pair-wise comparisons were made using orthogonal contrast statements, with p-values adjusted using the Holm test to maintain family-wise alpha at 0.05. Sensorimotor testing details are described in Supplemental Methods.

Supplementary Material

Refer to Web version on PubMed Central for supplementary material.

ACKNOWLEDGEMENTS

This work was supported by the Department of Defense Congressionally-Directed Medical Research Program award (TS100067 and TS110083, MZ). Additional support includes: Brown Institute for Brain Science (EAN, CIM), NIH NSGP training grant (NS062443-02, EAN), NIH/NIMH Conte Center grant (P50 MH086400-03, BWC), EFRI-BioSA/NSF (BWC), NIH (7-R01NS045130-08, CIM). MZ and EAN conceived of the project and wrote the manuscript. MZ oversaw all experiments and analysis. EAN conducted and oversaw primary experiments and data analysis. SC conducted and analyzed whole-cell electrophysiology data with EAN. CAT and EMM conducted and analyzed LFPs. CIM and BWC consulted on electrophysiology experimental design and analysis. JTM conducted biostatistics with EAN and MZ. CB analyzed grooming and seizures under the supervision of EAN and MZ. BV performed barrel analysis with EAN and MZ. Sensorimotor function was tested and analyzed by K. Bath (rndb.clps.brown.edu). We thank S. Cruikshank for his help with the lentiviral experiments.

REFERENCES

Agmon A, Connors BW. Thalamocortical responses of mouse somatosensory (barrel) cortex in vitro. Neuroscience. 1991; 41:365–379. [PubMed: 1870696]

Au KS, Hebert AA, Roach ES, Northrup H. Complete inactivation of the TSC2 gene leads to formation of hamartomas. Am. J. Hum. Genet. 1999; 65:1790–1795. [PubMed: 10577937]

Blumenfeld H. From Molecules to Networks: Cortical/Subcortical Interactions in the Pathophysiology of Idiopathic Generalized Epilepsy. 2003:1–9.

Brown A, Brown S, Ellisor D, Hagan N, Normand E, Zervas M. A practical approach to genetic inducible fate mapping: a visual guide to mark and track cells in vivo. J Vis Exp. 2009

Carson RP, Van Nielen DL, Winzenburger PA, Ess KC. Neuronal and glia abnormalities in Tsc1-deficient forebrain and partial rescue by rapamycin. Neurobiology of Disease. 2012; 45:369–380. [PubMed: 21907282]

Casper KB, McCarthy KD. GFAP-positive progenitor cells produce neurons and oligodendrocytes throughout the CNS. Molecular and Cellular Neuroscience. 2006; 31:676–684. [PubMed: 16458536]

Chen L, Guo Q, Li JYH. Transcription factor Gbx2 acts cell-nonautonomously to regulate the formation of lineage-restriction boundaries of the thalamus. Development. 2009; 136:1317–1326. [PubMed: 19279136]

Choi YJ, Di Nardo A, Kramvis I, Meikle L, Kwiatkowski DJ, Sahin M, He X. Tuberous sclerosis complex proteins control axon formation. Genes & Development. 2008; 22:2485–2495. [PubMed: 18794346]

Cohen I, Attwell D, Strichartz G. The dependence of the maximum rate of rise of the action potential upstroke on membrane properties. Proc. R. Soc. Lond., B, Biol. Sci. 1981; 214:85–98. [PubMed: 6121330]

Crino PB, Aronica E, Baltuch G, Nathanson KL. Biallelic TSC gene inactivation in tuberous sclerosis complex. American Academy of Neurology. 2010; 74:1716–1723.

Cromwell HC, Berridge KC. Implementation of action sequences by a neostriatal site: a lesion mapping study of grooming syntax. J. Neurosci. 1996; 16:3444–3458. [PubMed: 8627378]

Cruikshank SJ, Ahmed OJ, Stevens TR, Patrick SL, Gonzalez AN, Elmaleh M, Connors BW. Thalamic Control of Layer 1 Circuits in Prefrontal Cortex. Journal of Neuroscience. 2012; 32:17813–17823. [PubMed: 23223300]

Cruikshank SJ, Urabe H, Nurmikko AV, Connors BW. Pathway-specific feedforward circuits between thalamus and neocortex revealed by selective optical stimulation of axons. Neuron. 2010; 65:230–245. [PubMed: 20152129]

Ellisor D, Koveal D, Hagan N, Brown A, Zervas M. Comparative analysis of conditional reporter alleles in the developing embryo and embryonic nervous system. Gene Expression Patterns. 2009; 9:475–489. [PubMed: 19616131]

Fitzgerald KD, Welsh RC, Stern ER, Angstadt M, Hanna GL, Abelson JL, Taylor SF. Developmental alterations of frontal-striatal-thalamic connectivity in obsessive-compulsive disorder. J Am Acad Child Adolesc Psychiatry. 2011; 50:938–948. e3. [PubMed: 21871375]

Goto J, Talos DM, Klein P, Qin W, Chekaluk YI, Anderl S, Malinowska IA, Di Nardo A, Bronson RT, Chan JA, et al. Regulable neural progenitor-specific Tsc1 loss yields giant cells with organellar dysfunction in a model of tuberous sclerosis complex. Proc. Natl. Acad. Sci. U.S.a. 2011; 108:E1070–E1079. [PubMed: 22025691]

Hall JG. Review and hypotheses: somatic mosaicism: observations related to clinical genetics. Am. J. Hum. Genet. 1988; 43:355–363. [PubMed: 3052049]

Hardan AY, Minshew NJ, Melhem NM, Srihari S, Jo B, Bansal R, Keshavan MS, Stanley JA. An MRI and proton spectroscopy study of the thalamus in children with autism. Psychiatry Research: Neuroimaging. 2008; 163:97–105. [PubMed: 18508243]

Hay N. Upstream and downstream of mTOR. Genes & Development. 2004; 18:1926–1945. [PubMed: 15314020]

Hentges KE, Sirry B, Gingeras AC, Sarbassov D, Sonenberg N, Sabatini D, Peterson AS. FRAP/mTOR is required for proliferation and patterning during embryonic development in the mouse. Proc. Natl. Acad. Sci. U.S.a. 2001; 98:13796–13801. [PubMed: 11707573]

John A, Wildner H, Britsch S. The homeodomain transcription factor Gbx1 identifies a subpopulation of late-born GABAergic interneurons in the developing dorsal spinal cord. Dev. Dyn. 2005; 234:767–771. [PubMed: 16193514]

Knox S, Ge H, Dimitroff BD, Ren Y, Howe KA, Arsham AM, Easterday MC, Neufeld TP, O'Connor MB, Selleck SB. Mechanisms of TSC-mediated Control of Synapse Assembly and Axon Guidance. PLoS ONE. 2007; 2:e375. [PubMed: 17440611]

Kwiatkowski DJ, Zhang H, Bandura JL, Heiberger KM, Glogauer M, el-Hashemite N, Onda H. A mouse model of TSC1 reveals sex-dependent lethality from liver hemangiomas, and up-regulation of p70S6 kinase activity in Tsc1 null cells. Human Molecular Genetics. 2002; 11:525–534. [PubMed: 11875047]

Landisman CE, Connors BW. VPM and PoM Nuclei of the Rat Somatosensory Thalamus: Intrinsic Neuronal Properties and Corticothalamic Feedback. Cerebral Cortex. 2007; 17:2853–2865. [PubMed: 17389627]

Luu B, Ellisor D, Zervas M. The lineage contribution and role of Gbx2 in spinal cord development. PLoS ONE. 2011; 6:e20940. [PubMed: 21698205]

Madisen L, Zwingman TA, Sunkin SM, Oh SW, Zariwala HA, Gu H, Ng LL, Palmiter RD, Hawrylycz MJ, Jones AR, et al. A robust and high-throughput Cre reporting and characterization system for the whole mouse brain. Nat Neurosci. 2010; 13:133–140. [PubMed: 20023653]

McClintock WM. Neurologic manifestations of tuberous sclerosis complex. Curr Neurol Neurosci Rep. 2002; 2:158–163. [PubMed: 11898483]

Meikle L, Pollizzi K, Egnor A, Kramvis I, Lane H, Sahin M, Kwiatkowski DJ. Response of a Neuronal Model of Tuberous Sclerosis to Mammalian Target of Rapamycin (mTOR) Inhibitors: Effects on mTORC1 and Akt Signaling Lead to Improved Survival and Function. Journal of Neuroscience. 2008; 28:5422–5432. [PubMed: 18495876]

Meikle L, Talos DM, Onda H, Pollizzi K, Rotenberg A, Sahin M, Jensen FE, Kwiatkowski DJ. A Mouse Model of Tuberous Sclerosis: Neuronal Loss of Tsc1 Causes Dysplastic and Ectopic Neurons, Reduced Myelination, Seizure Activity, and Limited Survival. Journal of Neuroscience. 2007; 27:5546–5558. [PubMed: 17522300]

Molnár Z, Adams R, Blakemore C. Mechanisms underlying the early establishment of thalamocortical connections in the rat. J. Neurosci. 1998; 18:5723–5745. [PubMed: 9671663]

Narboux-Neme N, Evrard A, Ferezou I, Erzurumlu RS, Kaeser PS, Laine J, Rossier J, Ropert N, Sudhof TC, Gaspar P. Neurotransmitter Release at the Thalamocortical Synapse Instructs Barrel Formation But Not Axon Patterning in the Somatosensory Cortex. Journal of Neuroscience. 2012; 32:6183–6196. [PubMed: 22553025]

Nie D, Di Nardo A, Han JM, Baharanyi H, Kramvis I, Huynh T, Dabora S, Codeluppi S, Pandolfi PP, Pasquale EB, et al. Tsc2-Rheb signaling regulates EphA-mediated axon guidance. Nat Neurosci. 2010; 13:163–172. [PubMed: 20062052]

Pan WX, Mao T, Dudman JT. Inputs to the dorsal striatum of the mouse reflect the parallel circuit architecture of the forebrain. Front Neuroanat. 2010; 4:147. [PubMed: 21212837]

Peça J, Feliciano C, Ting JT, Wang W, Wells MF, Venkatraman TN, Lascola CD, Fu Z, Feng G. Shank3 mutant mice display autistic-like behaviours and striatal dysfunction. Nature. 2011; 472:437–442. [PubMed: 21423165]

Raab-Graham KF, Haddick PCG, Jan YN, Jan LY. Activity- and mTOR-Dependent Suppression of Kv1.1 Channel mRNA Translation in Dendrites. Science. 2006; 314:144–148. [PubMed: 17023663]

Reith RM, McKenna J, Wu H, Hashmi SS, Cho S-H, Dash PK, Gambello MJ. Loss of Tsc2 in Purkinje cells is associated with autistic-like behavior in a mouse model of tuberous sclerosis complex. Neurobiology of Disease. 2013; 51:93–103. [PubMed: 23123587]

Ridler K, Suckling J, Higgins N, de Vries P, Stephenson C, Bolton P, Bullmore E. Neuroanatomical Correlates of Memory Deficits in Tuberous Sclerosis Complex. Cerebral Cortex. 2006; 17:261–271. [PubMed: 16603714]

Saalmann YB, Kastner S. Cognitive and perceptual functions of the visual thalamus. Neuron. 2011; 71:209–223. [PubMed: 21791281]

Schwaller B. Cytosolic Ca2+ buffers. Cold Spring Harb Perspect Biol. 2010; 2:a004051. [PubMed: 20943758]

She W-C, Quairiaux C, Albright MJ, Wang Y-C, Sanchez DE, Chang P-S, Welker E, Lu H-C. Roles of mGluR5 in synaptic function and plasticity of the mouse thalamocortical pathway. European Journal of Neuroscience. 2009; 29:1379–1396. [PubMed: 19519626]

Shmelkov SV, Hormigo A, Jing D, Proenca CC, Bath KG, Milde T, Shmelkov E, Kushner JS, Baljevic M, Dincheva I, et al. Slitrk5 deficiency impairs corticostriatal circuitry and leads to obsessive-compulsive–like behaviors in mice. Nature Medicine. 2010; 16:598–602.

Smith Y, Raju DV, Pare J-F, Sidibe M. The thalamostriatal system: a highly specific network of the basal ganglia circuitry. Trends in Neurosciences. 2004; 27:520–527. [PubMed: 15331233]

Soriano P. Generalized lacZ expression with the ROSA26 Cre reporter strain. Nat. Genet. 1999; 21:70–71. [PubMed: 9916792]

Tsai PT, Hull C, Chu Y, Greene-Colozzi E, Sadowski AR, Leech JM, Steinberg J, Crawley JN, Regehr WG, Sahin M. Autistic-like behaviour and cerebellar dysfunction in Purkinje cell Tsc1 mutant mice. Nature. 2012:1–6.

Uhlmann EJ, Wong M, Baldwin RL, Bajenaru ML, Onda H, Kwiatkowski DJ, Yamada K, Gutmann DH. Astrocyte-specific TSC1 conditional knockout mice exhibit abnormal neuronal organization and seizures. Ann Neurol. 2002; 52:285–296. [PubMed: 12205640]

Way SW, McKenna J, Mietzsch U, Reith RM, Wu HC-J, Gambello MJ. Loss of Tsc2 in radial glia models the brain pathology of tuberous sclerosis complex in the mouse. Human Molecular Genetics. 2009; 18:1252–1265. [PubMed: 19150975]

Welch JM, Lu J, Rodriguiz RM, Trotta NC, Peça J, Ding J-D, Feliciano C, Chen M, Adams JP, Luo J, et al. Cortico-striatal synaptic defects and OCD-like behaviours in Sapap3-mutant mice. Nature. 2007; 448:894–900. [PubMed: 17713528]

Wimmer VC, Bruno RM, de Kock CPJ, Kuner T, Sakmann B. Dimensions of a projection column and architecture of VPM and POm axons in rat vibrissal cortex. Cerebral Cortex. 2010; 20:2265–2276. [PubMed: 20453248]

Wong V, Khong P-L. Tuberous sclerosis complex: correlation of magnetic resonance imaging (MRI) findings with comorbidities. J. Child Neurol. 2006; 21:99–105. [PubMed: 16566871]

Wong-Riley MT, Welt C. Histochemical changes in cytochrome oxidase of cortical barrels after vibrissal removal in neonatal and adult mice. Proc. Natl. Acad. Sci. U.S.a. 1980; 77:2333–2337. [PubMed: 6246540]

Woolsey TA, Van der Loos H. The structural organization of layer IV in the somatosensory region (SI) of mouse cerebral cortex. The description of a cortical field composed of discrete cytoarchitectonic units. Brain Res. 1970; 17:205–242. [PubMed: 4904874]

Zervas M, Somers KL, Thrall MA, Walkley SU. Critical role for glycosphingolipids in Niemann-Pick disease type C. Curr. Biol. 2001; 11:1283–1287. [PubMed: 11525744]

HIGHLIGHTS

1. Spatially and temporally controlled *Tsc1* deletion mimics genetic mosaicism
2. Early *Tsc1* deletion causes abnormal thalamic neuron physiology
3. *Tsc1* mutant thalamic circuits alter somatosensory cortex patterning and function
4. *Tsc1* deletion within developing thalamus causes abnormal grooming and seizures

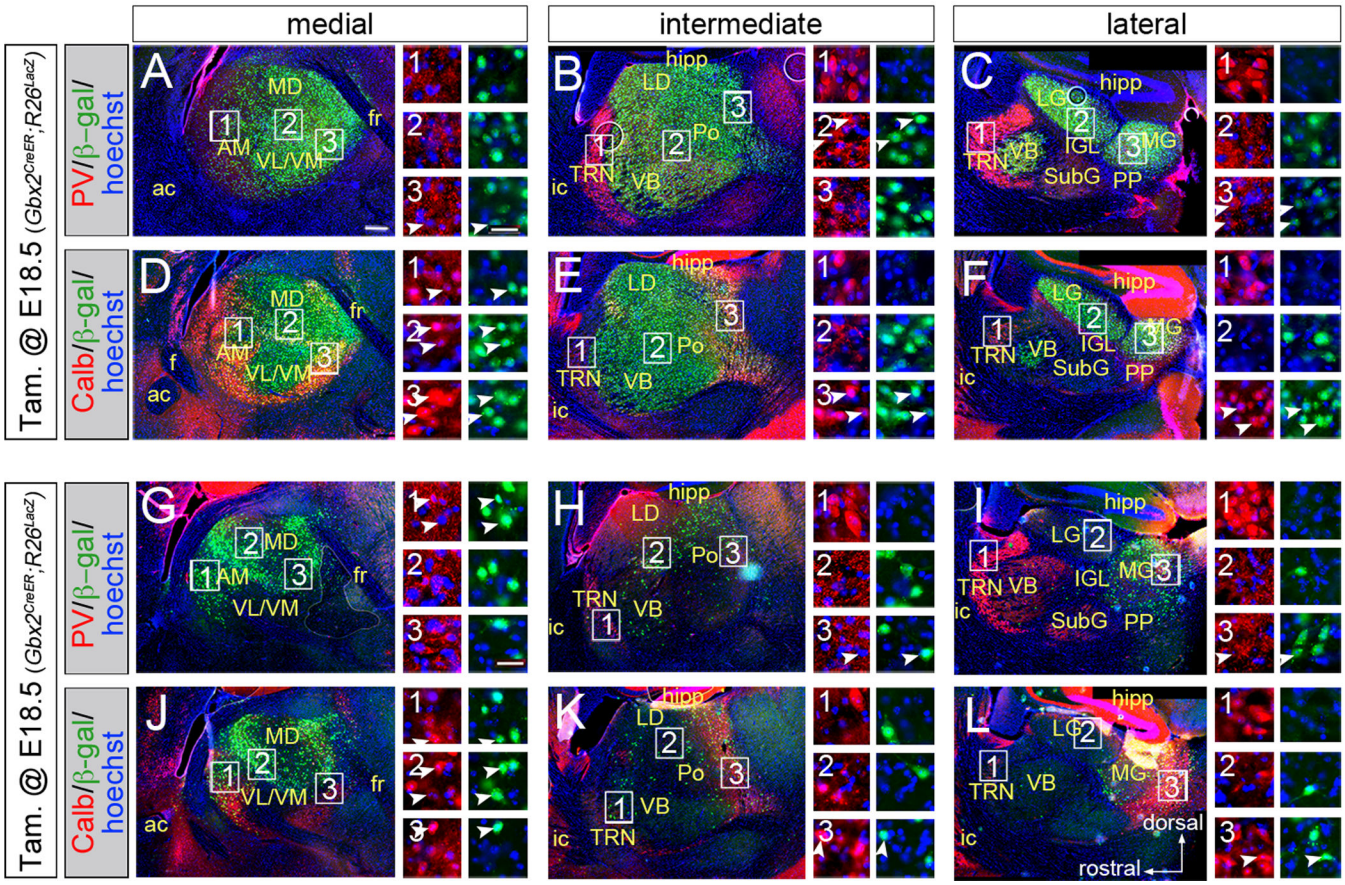

Figure 1. *Gbx2*^{CreER}-mediated thalamic recombination in thalamic neurons

(A–F) Expression of β-gal (green) in sagittal sections of thalamus. Co-localization with parvalbumin (PV, red, A–C) or calbindin (Calb, red, D–F) is indicated by arrowheads. (G–L) Recombination in PV+ (G–I) or Calb+ (J–L) neurons. Scale bar in A (270μm) applies to low-magnification panels; scale bar in A3 (30μm) applies to high magnification panels. Thalamic nuclei: anteromedial (AM), laterodorsal (LD), lateral geniculate (LG), mediodorsal (MD), medial geniculate (MG), posterior (Po), peripeduncular (PP), subgeniculate (SubG), thalamic reticular (TRN), ventrobasal (VB), ventrolateral (VL), ventromedial (VM). Additional abbreviations: anterior commissure (a.c.), fornix (f), fasciculus retroflexus (fr), hippocampus (hipp), internal capsule (i.c.), intergeniculate leaflet (IGL); See also Figure S1.

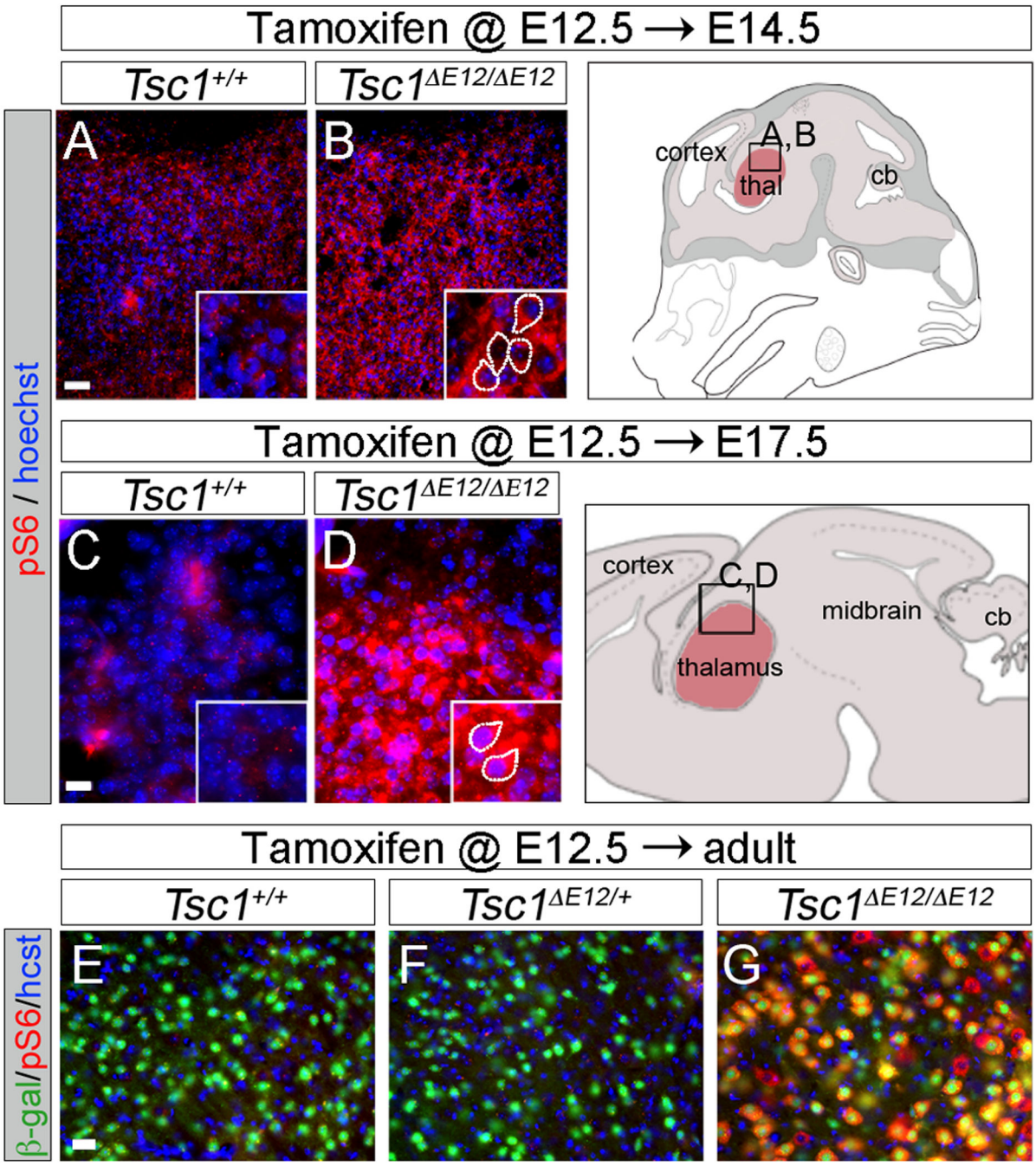

Figure 2. Conditional deletion of *Tsc1* in the thalamus causes rapid mTOR dysregulation

(A,B) pS6 (red) immunolabeling in E14.5 *Tsc1*$^{\Delta E12/\Delta E12}$ embryos. (C,D) E17.5 *Tsc1*$^{\Delta E12/\Delta E12}$ embryos had a robust increase in pS6 (red) compared to controls. (E–G) *Tsc1*$^{\Delta E12/\Delta E12}$ mutants had high pS6 levels (red). *R26*^{LacZ} (β-gal, green) independently showed similar recombination efficiency across genotypes. Control and mutant sections were imaged with identical exposure settings. n≥3 animals per genotype per stage. Scale bars: (A,B) 30μm, (C,D) 15μm, (E–G) 30μm.

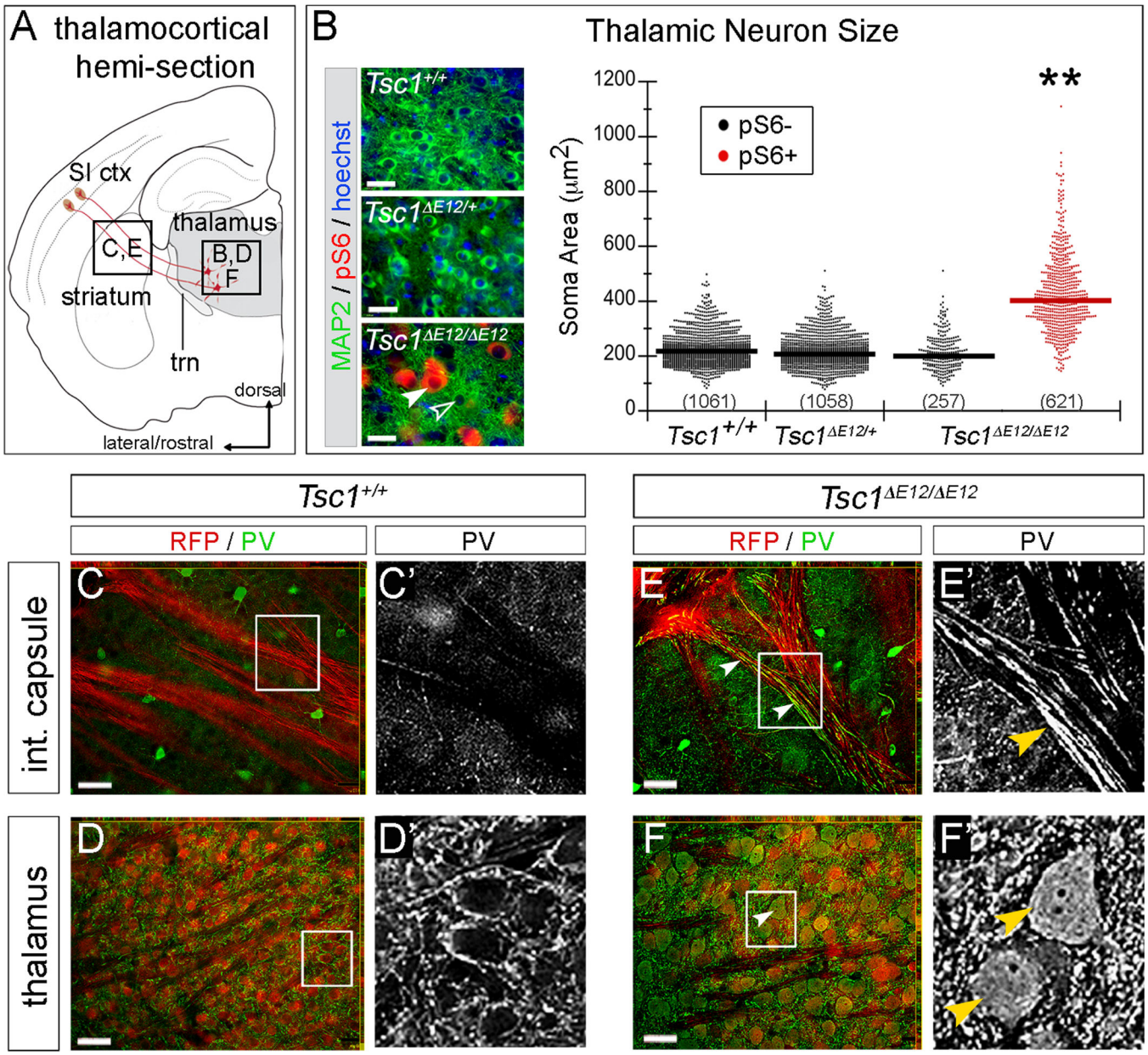

Figure 3. Cellular phenotypes caused by *Tsc1* deletion in thalamus at E12.5

(A) Thalamocortical regions of interest. (B) Sections were immunolabeled for MAP2 (green), pS6 (red), and counterstained with Hoechst (blue). Thalamic neurons of $Tsc1^{+/+}$ and $Tsc1^{\Delta E12/+}$ mice were pS6-. Recombination produced a mosaic thalamus of unaffected (pS6-, open arrowhead) and affected (pS6+, filled arrowhead) neurons. Soma area is plotted by genotype and pS6 status. Numbers of neurons are listed and geometric means indicated by horizontal lines. (C–F) Analysis of PV (green) and RFP (red) revealed PV+ fibers in the internal capsule of $Tsc1^{\Delta E12/\Delta E12}$ mice (E, arrowheads), but not in controls (C). Soma of $Tsc1^{\Delta E12/\Delta E12}$ RFP+ neurons were also PV+ (F, arrowheads). n=3 animals per genotype. Scale bars: (B) 32μm (C–F) 48μm. **p<0.005. See also Figure S2.

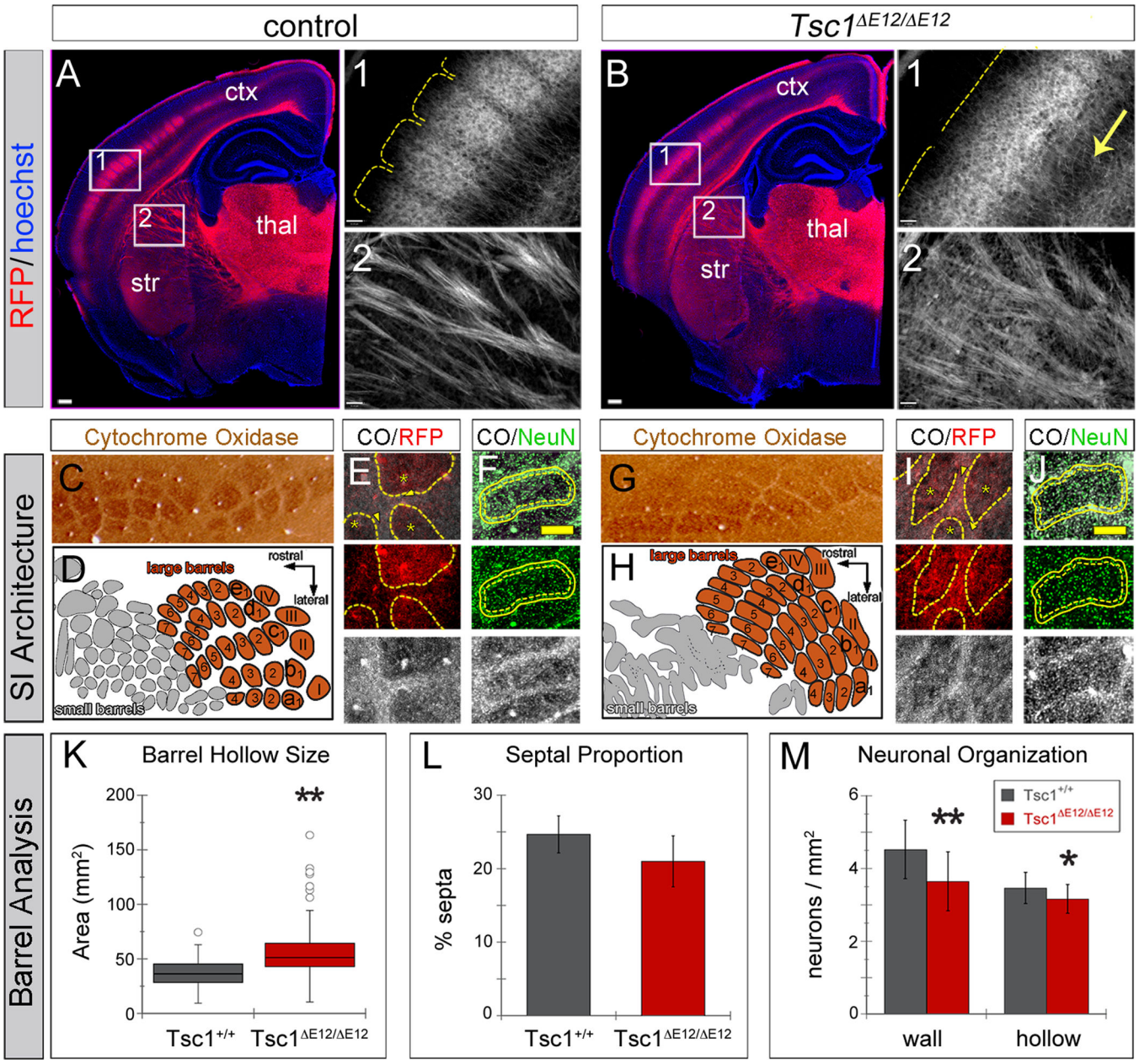

Figure 4. *Tsc1*$^{\Delta E12/\Delta E12}$ mutants have abnormal thalamocortical circuits

(A,B) RFP+ TCAs (red) delineated individual vibrissa barrels in *Tsc1*$^{+/+}$ neocortex, but were diffuse in *Tsc1*$^{\Delta E12/\Delta E12}$ mutants (region 1). Mutants had excess axonal processes in deep cortical layers (arrow) and RFP+ TCA fascicles that were less defined in the internal capsule (region 2). (C–J) Cortical vibrissa barrels stained with cytochrome oxidase (CO). (C,D) Controls had well-defined CO+ barrels (brown) separated by CO-septa. (G,H) *Tsc1*$^{\Delta E12/\Delta E12}$ cortex had misshapen barrels (brown) and small vibrissa barrels were nearly indistinguishable (gray). (E,I) *Tsc1*$^{+/+}$ RFP+ TCAs (red) targeted the CO+ barrel hollows (black, asterisks) but were less restricted in *Tsc1*$^{\Delta E12/\Delta E12}$ mice. (F,J) Barrel neurons (NeuN +, green) clustered around the perimeter of CO+ barrel hollows (black). Dashed line: extent of CO+ barrel hollow. Solid line: 15mm outer perimeter (“wall”) used for quantification in

M. (K) Average CO+ barrel size was larger in *Tsc1*$^{\Delta E12/\Delta E12}$ mutants. (L) The septa proportion showed no difference. (M) *Tsc1*$^{\Delta E12/\Delta E12}$ mice had lower neuron density in the barrel wall and hollow versus *Tsc1*$^{+/+}$ animals. Scale bars: (A,B) 240μm; (A1,A2,B1,B2) 61μm; (F,J) 130mm. thal, thalamus; str, striatum; ctx, neocortex. *p<0.05, **p<0.005. Data are represented as mean ± s.d. See also Figure S3.

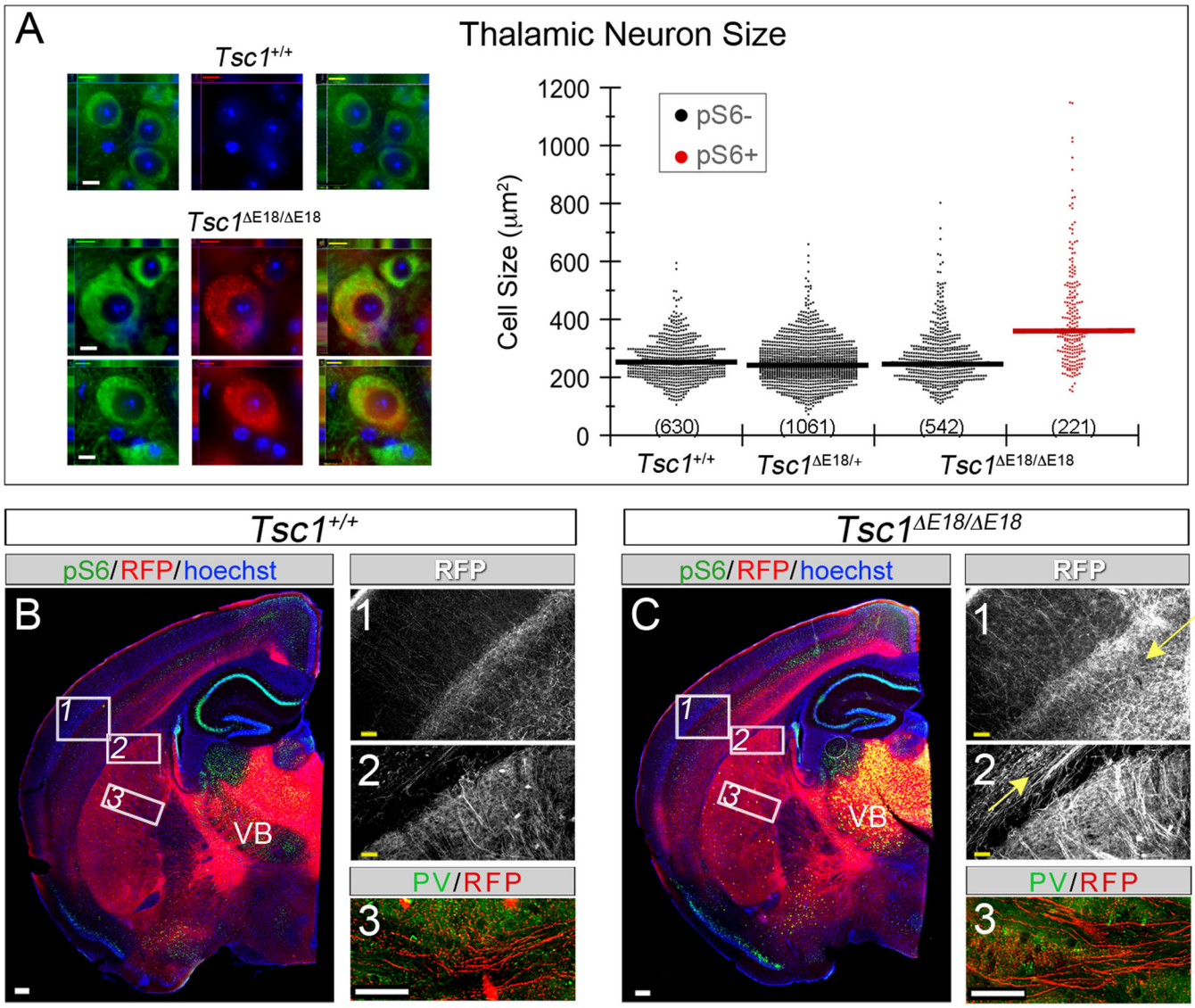

Figure 5. *Tsc1* deletion at E18.5 in the thalamus causes excessive thalamic axons

(A) Control and *Tsc1*$^{\Delta E18/\Delta E18}$ sections were immunostained for MAP2 (green) and pS6 (red). Soma size was graphed by genotype and pS6 expression and showed no significant difference. Note: pS6+ neurons were rarely observed in *Tsc1*$^{+/+}$ (2 cells) and *Tsc1*$^{\Delta E18/\Delta E18}$ brains (8 cells) and were not graphed for clarity. (B,C) *Tsc1*$^{+/+}$ and *Tsc1*$^{\Delta E18/\Delta E18}$ sections were immunolabeled for RFP (red) and pS6 (green). *Tsc1*$^{\Delta E18/\Delta E18}$ TCAs were superfluous and disorganized in deep cortical layers (region 1, arrow) and internal capsule (region 2, arrow). PV (region 3, green) was absent from *Tsc1*$^{\Delta E18/\Delta E18}$ and *Tsc1*$^{+/+}$ TCAs (red). Scale bars: (A) 8 μm (B,C) 240μm; (B1,B2,C1,C2) 61μm; (B3,C3) 57μm. See also Figure S4.

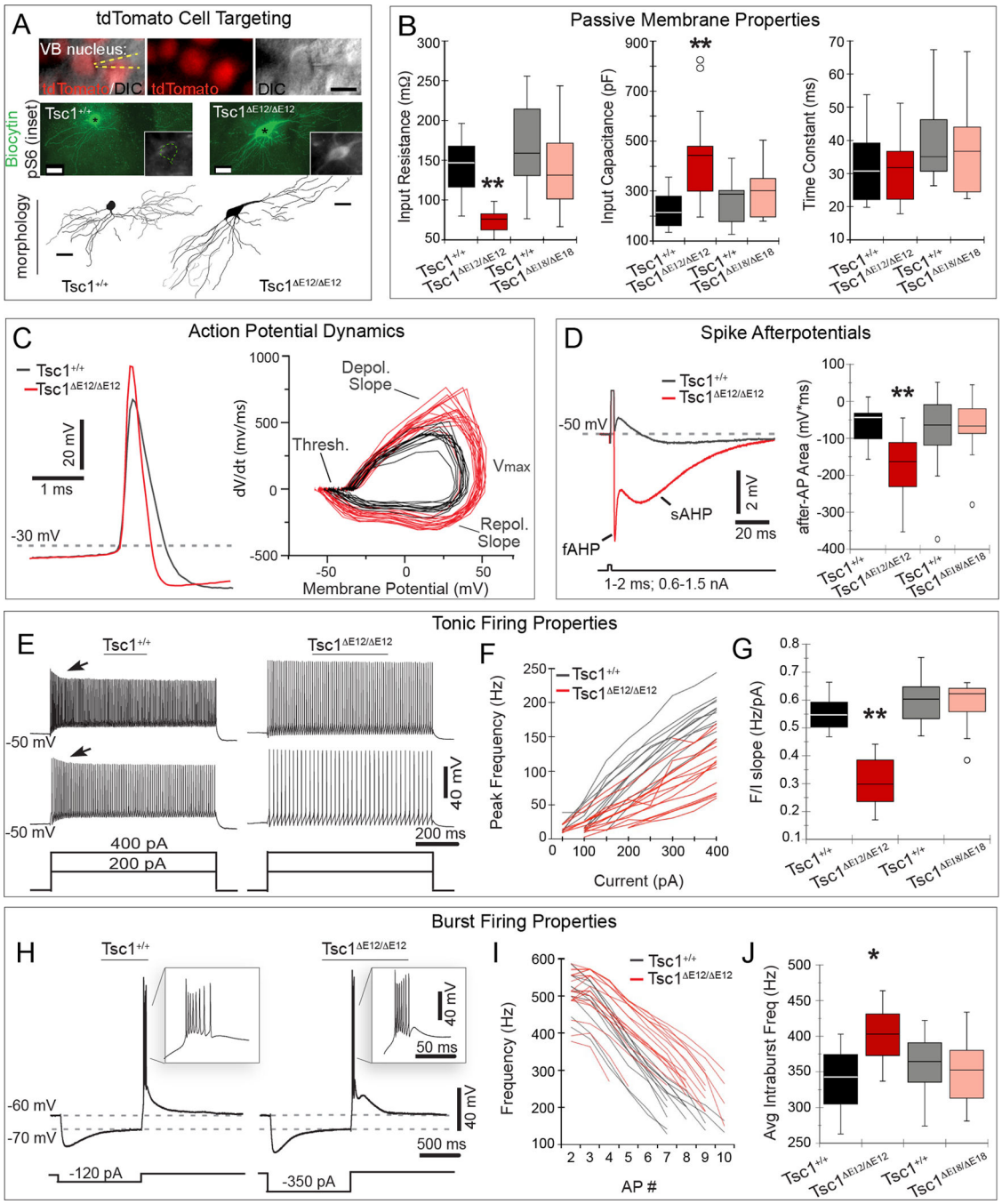

Figure 6. *Tsc1*$^{\Delta E12/\Delta E12}$ thalamic neurons have altered electrophysiological properties

(A) DIC/fluorescence shows electrode (yellow dashed lines) targeted to a RFP+ (red) VB neuron. Neurons were filled with biocytin (green) and immunostained for pS6 (white, insets). Morphology was reconstructed as shown below each filled neuron. (B) *Tsc1*$^{\Delta E12/\Delta E12}$ neurons (red) had lower membrane input resistance and higher input capacitance, but unchanged time constants compared to littermate controls (black), and to E18.5 mutants (pink) and controls (gray). (C) Representative traces from E12.5 control and mutant (left) shows that *Tsc1*$^{\Delta E12/\Delta E12}$ action potentials were faster and larger.

Tsc1$^{\Delta E12/\Delta E12}$ action potential dynamics (right) were significantly different with respect to depolarization rate, maximum amplitude, and repolarization rate. *Tsc1*$^{\Delta E18/\Delta E18}$ neurons were similar to controls (Figure S5). (D) *Tsc1*$^{\Delta E12/\Delta E12}$ spike afterpotentials (red) were more negative during the fast (fAHP) and during the slow phase (sAHP) compared to controls (black). Total post-spike membrane potential was integrated over time and quantified by integrating the voltage signal over 280 ms (right). (E) Representative tonic voltage response of a *Tsc1*$^{+/+}$ and *Tsc1*$^{\Delta E12/\Delta E12}$ neuron to current injections (400 pA, top and 200 pA, bottom). (F) Peak firing frequency per current step (F/I) is plotted for *Tsc1*$^{+/+}$ (black, n=12) and *Tsc1*$^{\Delta E12/\Delta E12}$ neurons (red, n=17) (G) Linear slopes of the F/I curves are quantified. (H) Representative voltage response of a *Tsc1*$^{+/+}$ and a *Tsc1*$^{\Delta E12/\Delta E12}$ thalamic neuron to hyperpolarizing current step. Insets show rebound bursts. (I) Intraburst firing frequency as a function of spike number within each burst is plotted for *Tsc1*$^{+/+}$ (black, n=11) and *Tsc1*$^{\Delta E12/\Delta E12}$ neurons (red, n=18). (J) Mean intraburst firing frequencies are quantified. Box plots represent minimum, first quartile (Q1), median, Q3, and maximum. Outliers (open circles) were >Q3+1.5*IQR or <Q1−1.5*IQR. Scale bars: (A) 20 μm (DIC), 30 μm (biocytin/morphology). *p<0.05, **p<0.005. See also Figure S5.

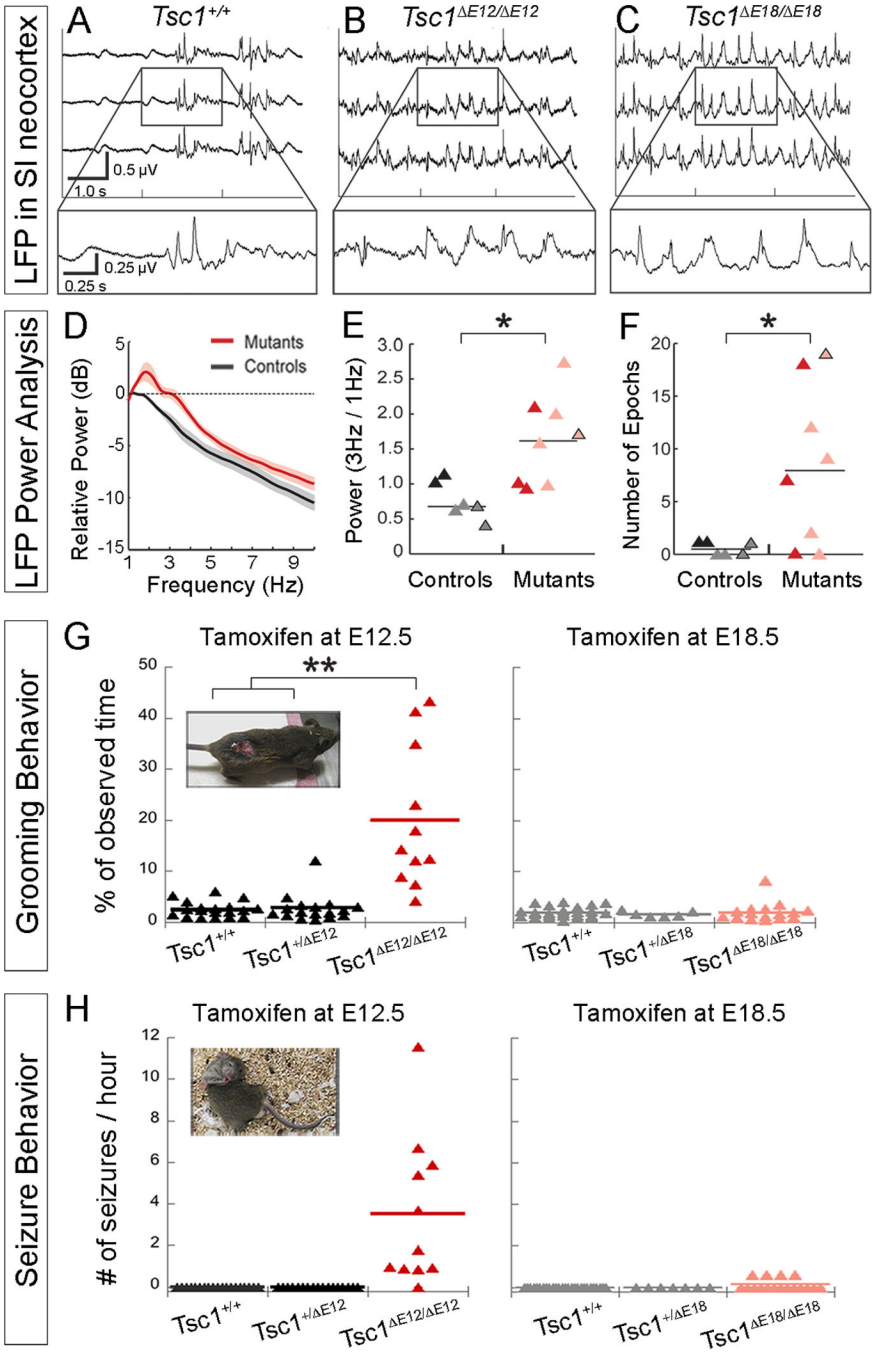

Figure 7. Abnormal brain activity and behaviors caused by thalamic *Tsc1* deletion

(A–C) LFPs in primary somatosensory neocortex were altered in *Tsc1*$^{\Delta E12/\Delta E12}$ and *Tsc1*$^{\Delta E18/\Delta E18}$ mutants. (D) Average power spectra of mutants and controls (E12.5 and E18.5 experiments were pooled together) shows increased power between 2–4Hz. Lines and shading represent mean ± SEM (E) 3Hz power was normalized to 1Hz power for controls (black, E12.5; gray, E18.5) and mutants (red, *Tsc1*$^{\Delta E12/\Delta E12}$; pink, *Tsc1*$^{\Delta E18/\Delta E18}$). Data points with black outlines represent recordings performed on aged animals (>8 months). (F) ≥20-second epochs of high-power 3Hz activity are plotted. (G) The percentage of time spent

grooming is plotted by genotype. E12.5 and E18.5 graphs share a y-axis. Inset: A *Tsc1*$^{\Delta E12/\Delta E12}$ mouse that developed a wound from over-grooming (H) Number of seizures per hour of observation time is plotted by genotype. E12.5 and E18.5 graphs share a y-axis. Inset: Contorted posture typically observed during seizures. *$p<0.05$, **$p<0.005$. See also Figure S6.